Cu atoms and $(CH_3)_3CCN$ and CH_3CN give two adducts with ρ_M = 0.14–0.2 which are similar to two of the species given by Cu atoms and HCN,[3] and the third species formed with HCN is not observed with the alkyl cyanides. These species could be the cis and trans organocopper iminyls RC(Cu)=N̈ although we cannot eliminate the possibility that one of them has the bridged structure III or the imidoyl structure II. Interestingly C_6H_5CN, which might be expected to give a rather stable imidoyl, does not give an identifiable adduct with Cu. CH_2CHCN, on the other hand, gives an adduct with a low ρ_M suggesting that it is not an iminyl although its exact structure is difficult to ascertain.

Conclusions. Group 11 metal atoms react with alkyl cyanides at 77 K in a rotating cryostat to give a variety of paramagnetic monoligand π-complexes and adducts. Complex formation can occur with either side-on or end-on bonding between the ligand and metal atom although end-on bonding species are only observed with Ag atoms. We do not detect complexation with more than one ligand in contrast to the situation when Ag atoms are formed by electron capture by Ag^+ in CH_3CN.[21,22] Organometallic iminyls are observed for all the cyanides and metals, and it would appear that organometallic imidoyls are not stable under our experimental conditions. There is tentative evidence for the formation of cis and trans iminyls although a bridged structure for one of the species cannot be ruled out.

Acknowledgment. J.A.H. and B.M. thank NATO for a collaborative research grant. H.D. thanks SERC for a CASE studentship. We also thank SERC for financial aid toward the purchase of equipment.

Registry No. Cu[$(CH_3)_3CCN$], 94801-03-3; Ag[$(CH_3)_3CCN$] (side-on bonded), 94801-04-4; Ag[$(CH_3)_3CCN$] (end-on bonded), 94801-05-5; Au[$(CH_3)_3CCN$], 94801-06-6; Ag[CD_3CN] (side-on bonded), 94801-07-7; Ag[CD_3CN] (end-on bonded), 94801-08-8; Au[CD_3CN], 94801-09-9; Cu[C_6H_5CN], 94801-10-2; Ag[C_6H_5CN], 94801-11-3; Cu[HCN], 94801-12-4; Ag[HCN] (side-on bonded), 94801-13-5; Ag[HCN] (end-on bonded), 94801-14-6; $(CH_3)_3CC$-(Cu)=N̈, 94801-15-7; $(CH_3)_3CC$(Ag)=N̈, 94801-16-8; $(CH_3)_3CC$-(Au)=N̈, 94801-17-9; CH_3C(Cu)=N̈, 94801-18-0; CD_3C(Ag)=N̈, 94801-19-1; CD_3C(Au)=N̈, 94801-20-4; C_6H_5C(Ag)=N̈, 94801-21-5; C_6H_5C(Au)=N̈, 94801-22-6; CH_2CHCN/Cu, 94801-23-7; CH_2CHCN/Ag, 94801-24-8; CH_iCHCN/Au, 94801-25-9.

(21) Symons, M. C. R.; Brown, D. R.; Eastland, G. W. *Chem. Phys. Lett.* **1979**, *61*, 91–95.

(22) Ichikawa, T.; Yoshida, H.; Li, A. S. W.; Kevan, L. *J. Am. Chem. Soc.* **1984**, *106*, 4324–4327.

C–H Activation. Synthesis of Silyl Derivatives of Niobocene and Tantalocene Hydrides, Their H/D Exchange Reactions with C_6D_6, and the Structure of $Cp_2Ta(H)_2SiMe_2Ph$

M. David Curtis,* Larry G. Bell, and William M. Butler

Department of Chemistry, The University of Michigan, Ann Arbor, Michigan 48109

Received June 26, 1984

Cp_2MH_3 (M = Nb, Ta) reacts with $PhMe_2SiH$ to give $Cp_2M(H)_2SiPhMe_2$. Cp_2NbH_3 reacts with pentamethyldisiloxane to give partial conversion to $Cp_2Nb(H)_2SiMe_2OSiMe_3$, and with Et_3SiH, no Nb silyl complexes were isolated. Cp_2NbH_3 catalyzes H/D exchange between Et_3SiH and C_6D_6 and produces deuterated $[Cp(\mu\text{-}\eta^1,\eta^5\text{-}C_5H_4)HNb]_2$, as the major organometallic product. Some general conclusions regarding productive activation of C–H bonds are drawn. The molecular structure of $Cp_2Ta(H)_2SiMe_2Ph$ was determined by X-ray crystallography: space group $P\bar{1}$, a = 7.856 (2) Å, b = 9.454 (2) Å, c = 12.257 (2) Å, α = 97.48 (2)°, β = 107.55 (1)°, γ = 98.09 (2)°, V = 845.1 (3) Å^3, Z = 2, ρ_{calcd} = 1.77 g/cm^3, R_1 = 0.036, R_2 = 0.046. The Ta–Si bond length is 2.651 (4) Å. Details of the ^{1}H NMR and the ^{93}Nb NMR of Cp_2NbH_3 are also reported.

Introduction

Activation of the C–H bond by transition-metal complexes is currently an area of intense research activity, and several important advances in this area have recently been reported.[1-3] In spite of the intense activity in this area, *productive* activation of the C–H bond by organometallic complexes is still a rare phenomenon. By a productive activation, we refer to a process wherein the hydrogen atom bonded to carbon is replaced with another functionality (this excludes H/D exchange) (eq 1). We are aware of only

$$\text{C–H} + \text{X–Y} \rightarrow \text{C–X} + \text{H–Y} \quad (1)$$

three examples of eq 1 being effected by discrete metal complexes in a homogeneous medium,[4] viz., eq 2–4.[1,3i,5]

$$\text{PhH} + \text{Et}_3\text{Al} \xrightarrow{Cp_2NbH_3} \text{Ph–AlEt}_2 + \text{Et–H} \quad (2)$$

$$\text{PhH} + \text{CO} \xrightarrow[h\nu]{(dppe)Ir(CO)H_3} \text{PhCHO} \quad (3)$$

$$\text{PhH} + \text{HSiR}_3 \xrightarrow{L_2Ir(CO)Cl} \text{Ph–SiR}_3 + \text{H}_2 \quad (4)$$

(1) Review of earlier work: Parshall, G. W. *Acc. Chem. Res.* **1975**, *8*, 113; *Catalysis* **1977**, *1*, 335.

(2) Theoretical treatment: Saillard, J.-Y.; Hoffmann, R. *J. Am. Chem. Soc.* **1984**, *106*, 2006.

(3) Leading references: (a) Fendrick, C. M.; Marks, T. J. *J. Am. Chem. Soc.* **1984**, *106*, 2214. (b) Crabtree, R. H.; Mihalais, J. M.; Quirk, J. M. *Ibid.* **1979**, *101*, 7748. (c) Watson, P. L. *Ibid.* **1983**, *105*, 6491. (d) Jones, W. D.; Feher, F. J. *Ibid.* **1984**, *106*, 1650. (e) Chamberlain, L. R.; Rothwell, A. P.; Rothwell, I. P. *Ibid.* **1984**, *106*, 1847. (f) Sweet, J. R.; Graham, W. A. G. *Ibid.* **1983**, *105*, 305. (g) Janowicz, A. H.; Bergman, R. G. *Ibid.* **1983**, *105*, 3929. (h) Kitajema, N.; Schwartz, J. *Ibid.* **1984**, *106*, 2220. (i) Fisher, G. J.; Eisenberg, R. *Organometallics* **1983**, *2*, 764. (j) Nemeh, S.; Jensen, C.; Binamira-Soriagi, E.; Kaska, W. C. *Ibid.* **1983**, *2*, 1442. (k) Green, M. A.; Huffman, J. C.; Caulton, K. G. *J. Am. Chem. Soc.* **1981**, *103*, 695. (l) Foust, D. F.; Rogers, R. D.; Rausch, M. D.; Atwood, J. L. *Ibid.* **1982**, *104*, 5646.

(4) A supported Rh complex also catalyzes the chlorination of methane. See reference 3h.

0276-7333/85/2304-0701$01.50/0

Scheme I

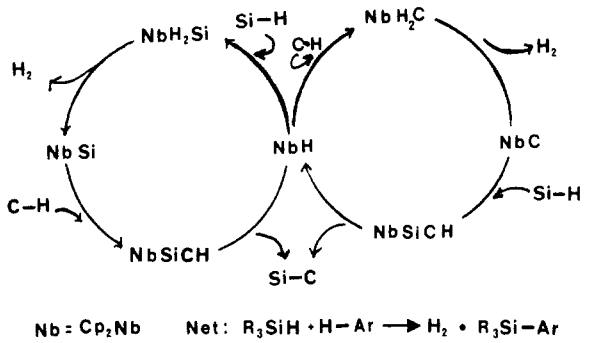

Equation 3 proceeds only under UV irradiation, and the total yield of phenylsilanes from eq 4 is very low since the major processes occurring in the system involve redistribution of groups on the silicon. In fact, the C–H activation depicted in eq 1 is nothing more than a redistribution or metathesis reaction and, as will be pointed out later (see Discussion), has many features in common with the redistribution of groups on silicon catalyzed by transition-metal complexes.[5-7]

Although $L_2Ir(CO)Cl$ (L = Ph_3P) is the catalyst precursor in eq 4, it is known that the iridium complex reacts rapidly with the excess silane to give R_3SiCl and $L_2Ir(CO)H$. The latter complex can then insert into Si–H, Si–C, and even Si–O bonds, as well as into the C–H bonds of the benzene solvent and at the ortho positions in the Ph_3P ligands.[6-8] The last possibility is expected to decrease the activity of the catalyst by diverting the metal species into a nonproductive cul-de-sac.

Parshall pointed out some time ago that a metal complex must possess three potentially exchangeable sites (or three potential sites of coordination) in order for the complex to catalyze a productive C–H activation according to eq 1. The iridium species in solution during the catalysis of the reaction shown in eq 4 apparently generates the required exchangeable sites by cycling among intermediates with the iridium in the +1 and +3 oxidation states.[5]

Since it had been demonstrated that Cp_2MH_3 (M = Nb, Ta) catalyze H/D exchange between H_2 and C_6H_6[1,9] (as well as the exchange depicted in eq 2) and since the reaction of silyl hydrides with Cp_2MH_3 had not been previously investigated, we undertook such an investigation with the expectation that these niobocene and tantalocene trihydrides would catalyze the H/Si exchange on benzene as shown in Scheme I. Furthermore, one of the starting materials, Cp_2NbH_3, exhibits highly unusual ^1H NMR behavior, and, although this has been mentioned previously,[9,10] we report here some detailed observations on the NMR behavior of this trihydride, as well as its ^{93}Nb NMR spectrum.

Experimental Section

General Procedure. All manipulations were performed under an atmosphere of argon using Schlenk techniques or in the nitrogen atmosphere of a drybox equipped with a purification train. Elemental analyses were carried out by Schwarzkopf Microanalytical Laboratory, Woodside, NY. Melting points were measured under nitrogen and are uncorrected. Proton NMR spectra were recorded on a Varian A-60 or a Bruker 360-MHz spectrometer. GC/mass spectra data were collected at 70 eV on a Finnigen 4023 GC/MS mass spectrometer. Infrared spectra were recorded on a Perkin-Elmer 457 spectrometer.

The silanes and siloxanes were purchased from Petrarch Systems, Inc., and were redistilled prior to use. Bu_3SnCp was prepared according to ref 11, vacuum distilled, and stored under N_2.

Cp_2MCl_2 (M = Nb, Ta). These compounds were prepared according to the literature method[12-14] from Bu_3SnCp and MCl_5 with this *important* modification: 3 equiv of Bu_3SnCp/equiv of MCl_5 must be used in order to obtain high yields of *pure* products. The use of 2 equiv of Bu_3SnCp/MCl_5 as described in ref 12–14 gives a mixture of Cp_2MCl_2 and $CpMCl_4$ which is difficult to separate into pure components, yield 85–90%.

Cp_2MH_3 (M = Nb, Ta). These were prepared according to the procedures of Green and Labinger[13-16] with modest modifications. To a suspension of 5.55 g (18.9 mmol) of Cp_2NbCl_2 in 100 mL of toluene at 0 °C was added 16.9 mL (57.5 mmol) of 3.4 M $NaAlH_2(OCH_2CH_2OMe)_2$ in toluene over a period of 16 min. The resulting brown solution was stirred at room temperature for 30 min, cooled to 0 °C, and hydrolyzed with 10 mL of degassed, distilled water. The toluene layer was extracted and filtered through a column of anhydrous Na_2SO_4 to give a yellow-brown solution. Removal of the solvent under vacuum gave a brown solid (mostly Cp_2NbH_3) in 85% yield. This solid shows a Nb–H absorption at 1660 cm^{-1} in addition to the Nb–H stretch due to Cp_2NbH_3 which occurs at 1700 cm^{-1}. The brown material also shows spurious resonances (δ ~4.75) in the Cp region (ca. 4% of the total Cp resonance). Sublimation of the brown material at 60 °C (10^{-3} torr) gave Cp_2NbH_3 (30% yield) as an off-white (very pale purple) solid which shows only one Nb–H (strong) (1700 cm^{-1}) and one Cp resonance (δ 4.75, 360 MHz, toluene-d_8).

Cp_2TaH_3 was prepared in an exactly analogous manner to give a very pale pink solid after sublimation. The ^1H NMR and IR spectra showed only bands due to the trihydride and were in agreement with those reported previously (δ –1.77 (t, 1 H), –3.12 (d, 2 H)).[9,10]

$Cp_2Nb(H)_2SiMe_2Ph$. Phenyldimethylsilane (546 mg, 4 mmol) was added to a solution of Cp_2NbH_3 (452 mg, 2 mmol) in 40 mL of toluene. After the solution was stirred at 55 °C for 3.5 h, the solvent was removed in vacuo, leaving a yellow-brown residue. The residue was extracted with 25 mL of *n*-hexane, and the resulting mixture was filtered to remove a small amount of a brown decomposition product. Cooling the solution to –20 °C produced 600 mg (83% yield) of yellow crystals: mp 106 °C; IR (Nujol) ν_{Nb-H} 1735 (b), 1305 (w), 1285 (w), 1250 (w), 1222 (m), 1075 (m), 1055 (m), 1005 (m), 995 (m), 905 (m), 810 (s), 790 (s), 770 (s), 730 (s), 690 (s), 672 (s), 655 (s), 625 (s), 470 (s) cm^{-1}; mass spectrum (70 eV), *m/e* 360 (1, M^+), 345 (0.9, $M^+ - CH_3$), 283 (0.5, $M^+ - C_6H_5$), 224 (29, $C_5H_5NbH^+$), 223 (30, $(C_5H_5)_2Nb$), 135 (57, $C_6H_5Si(CH_3)_2^+$), 121 (100, $H-Si(CH_3)(C_6H_5)^+$), 105 (26, $C_6H_5Si^+$), 58 (61, $Si(CH_3)_2$); NMR (360 MHz, toluene-d_6) δ 4.50 (s) (10 H, C_5H_5), 0.68 (s, 6 H, CH_3), –4.79 (2 H, NbH), 7.15–7.77 (5 H, phenyl multiplet). Anal. Calcd for $C_{18}H_{23}NbSi$: C, 60.00; H, 6.39. Found: C, 59.42; H, 6.59.

$Cp_2Ta(H)_2SiMe_2Ph$. This complex was prepared in a manner analogous to that of the Nb derivative, except that the reactants were heated to 110 °C for 12 h. Workup as above gave an 85% yield of product as pale yellow crystals: mp 116 °C; IR (Nujol) ν_{TaH} 1800 cm^{-1}; mass spectrum, *m/e* 448 (6.9, M^+), 446 (1, $M^+ - H_2$), 433 (15, $M^+ - CH_3$), 371 (1, $M^+ - C_6H_5$), 313 (13, $Cp_2TaH_2^+$), 312 (100, Cp_2TaH^+), 311 (19, Cp_2Ta^+), 135 (36, $(CH_3)_2Si(C_6H_5)^+$); NMR (360 MHz, toluene-d_8) δ 7.14–7.16 (m, 5 H, C_6H_5), 4.43 (s, 10 H, C_5H_5), 0.74 (s, 6 H, CH_3), –4.32 (s, 2 H, TaH). Anal. Calcd for $C_{18}H_{23}TaSi$: C, 48.21; H, 5.13. Found: C, 47.78; H, 5.13.

(5) Gustavson, W. A.; Epstein, P. S.; Curtis, M. D. *Organometallics* **1982**, *1*, 884.
(6) Curtis, M. D.; Epstein, P. S. *Adv. Organomet. Chem.* **1981**, *19*, 213.
(7) Gustavson, W. A.; Epstein, P. S.; Curtis, M. D. *J. Organomet. Chem.* **1982**, *238*, 87.
(8) Bell, L. G.; Gustavson, W. A.; Thanedar, S.; Curtis, M. D. *Organometallics* **1983**, *2*, 740.
(9) Tebbe, F. N.; Parshall, G. W. *J. Am. Chem. Soc.* **1971**, *93*, 3793.
(10) Labinger, J. A. *Compr. Organomet. Chem.* **1982**, *3*, 707, 770.
(11) Fritz, H. P.; Kreiter, C. G. *J. Organomet. Chem.* **1964**, *1*, 323.
(12) Bunker, M. J.; DeCian, A.; Green, M. L. H. *J. Chem. Soc., Chem. Commun.* **1977**, 59.
(13) Bunker, M. J.; DeCian, A.; Green, M. L. H.; Moreau, J. J. E.; Siganporia, N. *J. Chem. Soc. Dalton Trans.* **1980**, 2155.
(14) Labinger, J. A.; Wong, K. S. *J. Organomet. Chem.* **1979**, *170*, 373.
(15) Labinger, J. A.; Schwartz, J. *J. Am. Chem. Soc.* **1975**, *97*, 1596.
(16) Green, M. L. H.; Jousseaume, B. *J. Organomet. Chem.* **1980**, *193*, 339.

Table I. Crystal Data for $(\eta^5\text{-}C_5H_5)_2TaH_2Si(CH_3)_2(C_6H_5)$

space group $P\bar{1}$	mol wt = 448.4
a = 7.856 (2) Å	ρ(calcd) = 1.77 g cm^{-1}
b = 9.454 (2) Å	cryst dimens: 0.220 × 0.167 × 0.296 mm
c = 12.257 (2) Å	abs coeff: 65.04 cm^{-1}
α = 97.48 (2) deg	scan range, deg: Mo Kα − 0.8 to Mo Kα + 0.8
β = 107.55 (1) deg	2θ range, deg: 55
γ = 98.09 (2) deg	R_1 = 0.036 and R_2 = 0.046
V = 845.1 (3) Å^3	for 2623 reflections with $I > 3\sigma(I)$
Z = 2	total reflections = 4149

Table II. Temperature Dependence of the 360-MHz ^{1}H HNR Spectrum of the Metal-Bound Hydrogens of Cp_2NbH_3

			fwhm[b]		
T, °C	$\delta(H_a)$[a]	$\delta(H_b)$	H_a	H_b	$J(H_a)$[c]
28	−3.753	−2.746	17	39	11.16
19	−3.741	−2.734	17	34	9.00
10	−3.732	−2.724	11	39	6.12
0	−3.711	−2.701	7	37	1.44
−41	−3.700	−2.650	2	11	0.0

[a] Center of symmetric doublet if two peaks. [b] Full width (Hz) at half maximum height. [c] Separation (Hz) between the components of the doublet (apparent coupling constant, $J_{H_aH_b}$).

Reaction of Cp_2NbH_3 with $HSiMe_2OSiMe_3$. A solution of 113 mg (0.5 mmol) of Cp_2NbH_3 in 25 mL of C_6H_6 was allowed to react with 742 mg (5 mmol) of pentamethyldisiloxane. After 24 h at 60 °C, GC/MS analysis of the volatile components showed the presence of octamethyltrisiloxane (EDE), heptamethyltrisiloxane (E'DE), nonamethyltetrasiloxane (E'D$_2$E), and undecamethylpentasiloxane (E'D$_3$E) (E = $Me_3SiO_{1/2}$, E' = $Me_2HSiO_{1/2}$, D = $Me_2SiO_{2/2}$).

A preparative reaction was attempted with 226 mg (1 mmol) of Cp_2NbH_3 and 445 mg (3 mmol) of pentamethyldisiloxane in 40 mL of toluene at 60 °C. After 8 h, the solvent was removed and a green-brown residue was obtained. NMR analysis of the crude product indicated a mixture. Sublimation of the material at 60 °C (10^{-3} torr) gave a light brown product which the NMR spectrum showed was a mixture of the starting trihydride and $Cp_2Nb(H)_2(SiMe_2OSiMe_3)$.

H/D Exchange Studies. Appropriate quantities of C_6D_6 and reactants (Cp_2NbH_3, silane) were sealed under vacuum in NMR tubes on a vacuum line. The tubes were kept in a thermostated oil bath and removed periodically for ^{1}H NMR spectral measurements (60 MHz). Following the reactions, the tubes were cooled to −10 °C and opened in an inert-atmosphere box. The solid organometallic product was collected and analyzed by mass spectrometry and in one case by unit-cell determination on a Syntex P2$_1$ diffractometer.

X-ray Structure Determination of $Cp_2Ta(H)_2SiMe_2Ph$. Single crystals of the compound were grown by slow crystallization from a hexane solution at −20 °C. A crystal was mounted on a Syntex P2$_1$ diffractometer and the space group determined. Table I contains a summary of data collection conditions and results. Lattice parameters were determined from a least-squares refinement of 16 reflection settings obtained from an automatic centering routine.

Intensity data were obtained by using Mo Kα radiation monochromated from a graphite crystal whose diffraction vector was perpendicular to the diffraction vector of the sample. Three standard reflections were measured every 50 reflections. The data were reduced by procedures previously described.[17] An absorption correction was applied to the data. The structure was solved by using Patterson techniques. The function $\sum w(|F_o| - |F_c|)^2$ was minimized where $|F_o|$ and $|F_c|$ are the observed and calculated structure factor amplitudes. In the least-squares refinement, the agreement indices $R_1 = \sum||F_o| - |F_c||/\sum|F_o|$ and $R_2 = [\sum w(|F_o| - |F_c|)^2/\sum w|F_o|^2]^{1/2}$ were used. The atomic scattering factors are from ref 18.

Least-squares refinement using anisotropic thermal parameters for all non-hydrogen atoms gave R_1 = 0.038 and R_2 = 0.048. Positions for all hydrogen atoms connected to carbon atoms were calculated and added as fixed contributors. Refinement to convergence with all non-hydrogen atoms gave R_1 = 0.036 and R_2 = 0.046.

Final positional parameters with estimated standard deviations are shown in Table III. Anisotropic thermal parameters with their estimated standard deviations are listed in Table IV (supplementary), and Table V lists the crystallographically determined bond distances and angles. Listings of observed and calculated structure factor amplitudes are available as supplementary material (VI).

Table III. Fractional Atomic Coordinates for 4

atom	x	y	z
Ta	−0.00926 (3)	0.00476 (3)	0.24532 (2)
Si	0.1024 (3)	−0.2467 (2)	0.2541 (2)
C(1)	0.2956 (12)	0.0567 (12)	0.2506 (10)
C(2)	0.2780 (14)	0.1458 (16)	0.3450 (9)
C(3)	0.1624 (15)	0.2434 (12)	0.2973 (14)
C(4)	0.1103 (14)	0.2094 (14)	0.1795 (12)
C(5)	0.1918 (14)	0.0991 (14)	0.1504 (8)
C(6)	−0.2927 (11)	−0.1236 (11)	0.2452 (10)
C(7)	−0.3276 (11)	−0.0651 (13)	0.1431 (8)
C(8)	−0.2937 (11)	0.0793 (11)	0.1701 (9)
C(9)	−0.2375 (11)	0.1212 (10)	0.2862 (9)
C(10)	−0.2361 (12)	−0.0017 (15)	0.3375 (8)
C(11)	−0.0884 (10)	−0.3890 (8)	0.2573 (7)
C(12)	−0.2221 (12)	−0.4664 (9)	0.1560 (9)
C(13)	−0.3827 (14)	−0.5505 (10)	0.1575 (12)
C(14)	−0.4082 (15)	−0.5618 (11)	0.2607 (12)
C(15)	−0.2808 (16)	−0.4926 (12)	0.3634 (12)
C(16)	−0.1180 (13)	−0.4092 (10)	0.3610 (8)
C(17)	0.3053 (11)	−0.2532 (11)	0.3840 (8)
C(18)	0.1723 (14)	−0.3236 (11)	0.1260 (8)

Results and Discussion

Starting Materials. The most convenient route to the starting chlorides Cp_2MCl_2 uses the organotin reagent n-$Bu_3Sn(\sigma$-Cp) as a nonreductive source of the cyclopentadienide ion.[11] However, we have found that at least 3 equiv of Bu_3SnCp instead of the two as reported[12-14] are required to obtain pure samples of Cp_2MCl_2 in high yields (eq 5). When only 2 equiv of Bu_3SnCp are used, the

$$MCl_5 + 3Bu_3SnCp \xrightarrow{CH_2Cl_2} Cp_2MCl_2 + 3Bu_3SnCl + [C_5H_5\cdot] \quad (5)$$

product appears to consist of a mixture of Cp_2NbCl_2 and $CpNbCl_4$. Such a result is reasonable since 1 equiv of tin reagent is consumed in the reduction of M(V) to M(IV). Hence, the correct stoichiometry is as shown in eq 5.

Reduction of the dichlorides with $NaAlH_2(OCH_2CH_2OCH_3)_2$ (Vitride) followed by hydrolysis gives the trihydrides Cp_2MH_3.[13-16] The Cp_2NbH_3 product from these reductions has been variously described as brown to white. We have found that yellow to brown preparations show impurity bands in both the IR and NMR spectra. Careful sublimation at low pressure gives a nearly white solid which shows *only* bands assignable to Cp_2NbH_3 in the ^{1}H NMR spectrum. Even so, we suspect the off-white, purplish cast

(17) Computations were carried out on an Amdahl 470/V6 computer. Computer programs used during the structural analysis were SYNCOR (data reduction by W. Schmonsees), FORDAP (Fourier refinement by Z. Zalkin), ORFLS (full matrix, least-squares refinement by Busing, Martin, and Levy), ORFFE (distances, angles, and their esd's by Busing, Martin, and Levy), ORTEP (thermal ellipsoid drawings by C. K. Johnson), HATOMS (hydrogen atom positions by A. Zalkin), PLANES (least-squares planes by D. M. Blow), and ABSORB (absorption correction program by D. Templeton and L. Templeton).

(18) Ibers, J. A., Hamilton, W. C., Eds. "International Tables for X-Ray Crystallography"; Kynoch Press: Birmingham England, 1974, Vol. IV, Table 2.2 and Table 2.3.1.

Table V. Bond Distances (Å) and Angles (deg) for $(\eta^5\text{-}C_5H_5)_2Ta(H_2)Si(CH_3)_2(C_6H_5)$

Bond Distances

Ta-cent1	2.036 (7)	Ta-C(3)	2.360 (11)	Ta-C(6)	2.381 (9)
Ta-cent2	2.070 (7)	Ta-C(5)	2.371 (8)	Ta-C(7)	2.386 (8)
Ta-Si	2.651 (4)	Ta-C(4)	2.373 (10)	Ta-C(8)	2.389 (7)
Ta-C(2)	2.331 (10)	Ta-C(9)	2.373 (8)	C-C(Cp)	av 1.384 ± 0.035
Ta-C(1)	2.356 (9)	Ta-C(10)	2.378 (8)	C-C(Ph)	av 1.386 ± 0.023

Bond Angles

cent1-Ta-cent2	137.95 (19)	C-C-C(Cp)	av 108.0 ± 1.7	C(11)-C(12)-C(13)	122.4 (10)
Si-Ta-cent1	105.79 (21)	Ta-Si-C(17)	116.92 (26)	C(14)-C(13)-C(12)	119.5 (11)
Si-Ta-cent2	116.24 (20)	Ta-Si-C(18)	116.29 (24)	C(13)-C(14)-C(15)	121.3 (11)
C(11)-Si-C(17)	105.87 (39)	Ta-Si-C(11)	109.00 (23)	C-C-C(Ph)	av 120.0 ± 2.5
C(11)-Si-C(18)	105.23 (43)				
C(17)-Si-C(18)	102.47 (43)				

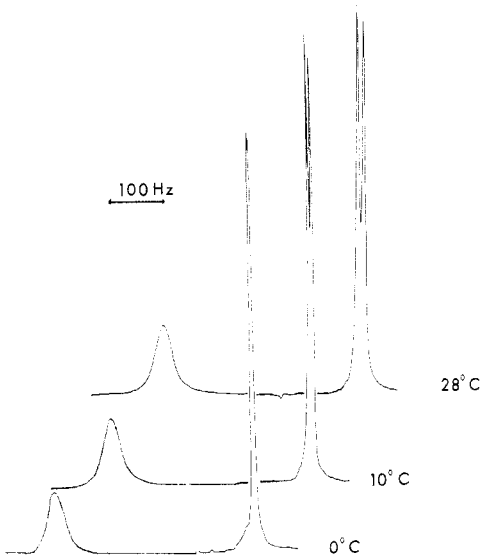

Figure 1. Metal hydride region of the 360-MHz ^1H NMR spectrum of Cp_2NbH_3 as a function of temperature.

to the solid is caused by trace amounts of highly colored impurities.

NMR Spectra. The ^1H NMR spectrum of Cp_2TaH_3 is straightforward and consists of a singlet for the Cp rings, a triplet for H_b, and a doublet for H_a. In contrast, the ^1H NMR spectrum of the niobium hydride 1 exhibits anom-

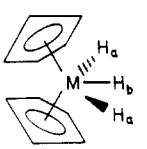

1, M = Nb
2, M = Ta

alies with respect to both temperature and magnetic field strength. The temperature dependence (Figure 1) has been noted previously,[9,10] but details of the temperature dependence have not been published. Below 0 °C, the resonance from H_a is a relatively sharp singlet. Between −41 and 0 °C, little change is noticed, but at 0 °C, the signal due to H_a begins to split into two peaks and the signal due to H_b begins to broaden. Table II describes the changes observed as a function of temperature.

The spectrum is also field dependent at constant temperature. Figure 2 shows the appearance of the spectrum at 60, 90, 360 MHz. As the field is lowered, the signal due to H_b broadens considerably, and at 60 MHz, it has disappeared into the base line. The two peaks shown for 60 MHz in Figure 2 correspond to the doublet due to H_a which is symmetric at 360 MHz. The H_a "doublet" has an intermediate appearance at 90 MHz. The fwhm values

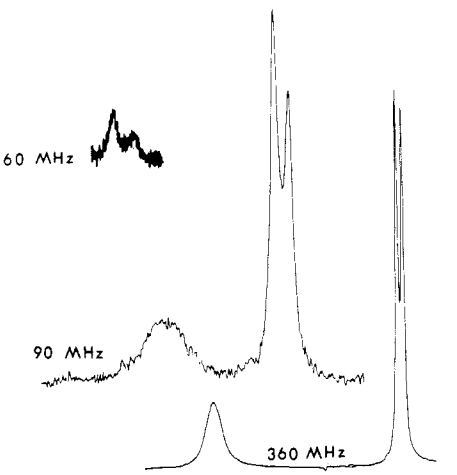

Figure 2. Metal hydride region of the ^1H NMR spectrum of Cp_2NbH_3 at various field strengths (T = 28 °C).

(ppm) are (in the order 360, 90, 60 MHz): 17, 24, and 22 for H_a and 39, 47, and not available for H_b.

Whitesides and Mitchell have performed an elegant study of the effects of ^{51}V quadrupolar relaxation on the spectrum of $(\eta\text{-}C_7H_7)V(CO)_3$.[19] At low temperature, where the rate of quadrupolar relaxation is fast, the ^1H NMR spectrum consists of a single line. As the temperature is increased, this signal broadens and eventually resembles an unresolved doublet. This apparent doublet is, however, an envelope of the eight lines expected from coupling of the protons to the ^{51}V nucleus ($I = {}^7/_2$).

Even though the shape of the "doublet" observed for Cp_2NbH_3 does not resemble the envelope expected for unresolved Nb–H coupling (^{93}Nb, $I = {}^9/_2$, Q = −0.22 barn), we have measured the ^{93}Nb NMR of Cp_2NbH_3 in order to determine its spin–lattice relaxation time (the appearance of the spectrum depends on T_1(Nb)—see ref 19). The Nb NMR appears as a very broad peak (fwhm = 800 ppm) at δ −2225 ppm upfield from $NbCl_6^{-1}$ in CH_3CN, taken as the standard (21.90 MHz, 30 °C). The relationship $\Delta\nu_{1/2} = 1/T_1$(Nb) gives a T_1 for Nb of ca. 2×10^{-5} s. This relaxation time is much too short to observe Nb–H coupling, and hence the appearance of the spectrum is not due to incompletely decoupled Nb–H coupling.

Having eliminated one possibility, we are at a loss to explain the spectrum. The fwhm of the peak due to H_b is roughly $3J(H_a) + 6$ for $T \geq 10$ °C (see Table II), which suggests that the peak for H_b is an unresolved triplet. Perhaps a difference in the Nb–H coupling constants between the inner and outer protons leads to a preferential broadening of the peaks due to the inner proton (H_b),[20]

(19) Whitesides, G. M.; Mitchell, H. L. *J. Am. Chem. Soc.* **1969**, *91*, 2245.

but the field and temperature dependence of the spectra require further work.

Silyl Complexes. Cp_2NbH_3 reacts readily with $PhMe_2SiH$ to give the silyl complex **3** (eq 6). The reaction

$$Cp_2NbH_3 + PhMe_2SiH \xrightarrow[3.5\ h.\ (-H_2)]{55\ °C} Cp_2Nb(H)SiMe_2Ph \quad (6)$$

3

presumably proceeds by reductive elimination of H_2 from the trihydride to give Cp_2NbH which then adds the silane. Complex **3** is isolated in an 80% yield as a yellow, crystalline solid, mp 106 °C. The complex is air sensitive, especially in solution.

The Nb–H stretch in **3** occurs as a single, broad peak at 1735 cm^{-1} (Nujol mull). The ^1H NMR spectrum of **3** is consistent with a time-averaged C_{2v} symmetry. The Nb–*H* signal appears as a singlet at δ −4.79, and the Cp rings and the SiMe groups are also equivalent and resonate at δ 4.50 and 0.68, respectively. Thus, the silicon replaces the central hydrogen as shown in **3**, and there is rapid rotation of the $PhMe_2Si$ group about the Nb–Si bond.

Cp_2TaH_3 also reacts with $PhMe_2SiH$ but higher temperatures and longer reaction times are necessary to effect complete conversion (eq 7). The spectral properties of

$$Cp_2TaH_3 + PhMe_2SiH \xrightarrow[12\ h.\ (-H_2)]{110\ °C} Cp_2Ta(H)SiMe_2Ph \quad (7)$$

4

4 resemble those of **3**: ν_{Ta-H} = 1800 cm^{-1} (br); ^1H NMR δ 4.43 (s, Cp), 0.74 (s, Me), −4.32 (s, TaH). The central attachment of the silyl group has been confirmed by a structure determination (see below). Compound **4** is a pale yellow solid, mp 116 °C. Both the solid and solutions of **4** are air sensitive.

Cp_2NbH_3 is a catalyst for the redistribution of groups on Si. Heating a solution of $HSiMe_2OSiMe_3$ and **1** (10:1) in benzene gave a low conversion of the pentamethyldisiloxane into higher polysiloxanes (eq 8). These higher

$$HSiMe_2OSiMe_3 \xrightarrow[60\ °C,\ 24\ h]{3} HSiMe_2(OSiMe_2)_nOSiMe_3 + (Me_3SiO)_2SiMe_3 \quad (8)$$
$$n = 1\text{–}3$$

polysiloxanes are the result of –H/–$OSiR_3$ and –Me/–$OSiR_3$ exchanges catalyzed by the metal species.[5-8] The mechanism presumably involves oxidative addition of a low-valent metal species into Si–H, Si–C, and Si–O bonds. Cp_2NbH_3 is not as effective a catalyst for this redistribution reaction as iridium or rhodium complexes.[5-8]

In a stoichiometric reaction (1:1 Cp_2NbH_3 and HMe_5Si_2O), the product isolated after 24 h at 60 °C was a mixture of **1** and the expected adduct $Cp_2Nb(H)_2SiMe_2OSiMe_3$. The more bulky triethylsilane Et_3SiH gave at most a low conversion to a silylniobium complex and, upon prolonged heating, the major product was the "niobocene" dimer $[Cp(\mu\text{-}\eta^1,\eta^5\text{-}C_5H_4)HNb]_2$ (**5**).[9,21] Thus, the order of reactivity of silyl hydrides toward **3** appears to be $PhMe_2SiH > Me_3SiOSiMe_2H > Et_3SiH$.

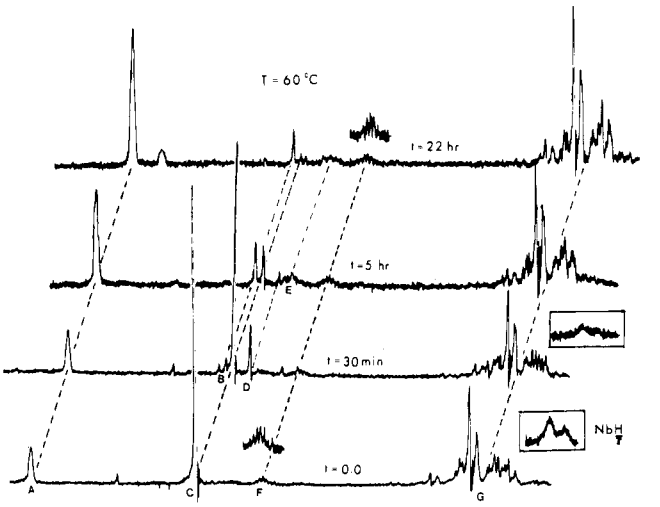

Figure 3. 60-MHz ^1H NMR spectra of a 10:1 mixture of Et_3SiH and Cp_2NbH_3 as a function of time (measurement temperature = 28 °C; reaction temperature = 60 °C).

H/D Exchange on C_6D_6 and R_3SiH. As mentioned in the introduction, we expected the complexes Cp_2MH_3 to catalyze the formation of phenylsilanes according to Scheme I. However, even though Cp_2NbH_3 catalyzes the exchange of groups on silicon, no phenylsiloxanes were observed when the reaction was conducted in benzene. In contrast, the iridium complex catalyzed reaction produces small yields of phenylsiloxanes (eq 4).[7] In order to determine if the C–H bonds of benzene were being attacked, several reactions of silanes with **1** were conducted in C_6D_6.

Heating a 1:10 mixture of **1** and $PhMe_2SiH$ in C_6D_6 to 60 °C for 16 h gave a quantitative conversion of **1** into **3** (NMR), and the excess $PhMe_2SiH$ was found to be ca. 2% monosubstituted with deuterium (MS) (eq 9).

$$PhMe_2SiH + \underset{10:1}{1} \xrightarrow{C_6D_6} 3 + \underset{\sim 2\%\ d_1}{PhMe_2SiH(D)} \quad (9)$$

However, more extensive H/D exchange was observed when a 10:1 mixture of Et_3SiH and **1** was heated to 60 °C for 22 h in C_6D_6. A series of ^1H NMR spectra obtained during the course of the reaction is shown in Figure 3. The peak marked A is due to residual protium in the C_6D_6. This peak monotonically increases in intensity while the peak marked C, due to Cp_2NbH_3, monotonically decreases in intensity. After 30 min, peaks B and D appear. Peak **B** grows to a maximum at t = 5 h and then decreases slightly, while peak D gradually disappears. After 5 h, an ill-resolved series of peaks E grow in and then diminish. Peak F is due to the Si–H proton, and G are the peaks due to the Et groups on Et_3SiH. The inset shows the diminution of the Nb–H signal; it is no longer evident after about 1 h.

It is apparent that some deuterium on benzene is replaced by some protium. Workup of the reaction mixture gave a nearly quantitative yield (>90%) of yellow air-stable crystals which were identified by MS and by determination of the unit cell parameters[21] to be deuterated niobocene dimer **5**. The recovered Et_3SiH was 20% d_1. In a separate run, the Et_3SiH was 51% d_1 after 16 h at 55 °C.[22]

(20) From the relationship, $\Delta\nu_{1/2}(H) = 1/\pi T_1(H_1) = {}^2/_3(2\pi J)^2 I(I+1)T_1(Nb)$, one can set upper limits to the Nb–H coupling constants at 28 °C. For H_a, the line width of each component of the doublet is ca. 6 Hz, so that $J(Nb\text{–}H_a) \leq \sim 40$ Hz. For H_b, if $\Delta\nu_{1/2}(H)$ is taken as 40 Hz, then $J(Nb\text{–}H_b) \leq \sim 100$ Hz.

(21) Guggenberger, L. J. *Inorg. Chem.* **1973**, *12*, 294.

(22) The rates of H/D exchange were erratic. The % deuteration of Et_3SiH was determined by computer matching of calculated spectra to the observed spectrum. It was not possible to determine the % deuteration of the dimer **5** due to extensive H loss from the parent ion. The envelope of peaks in the parent ion for the deuterated dimer spanned the range m/e 438–456 with maxima at m/e 448 and 449 (m/e for the undeuterated parent is at 446). Therefore **5**-d_n (n = 0–10) were detected.

Scheme II

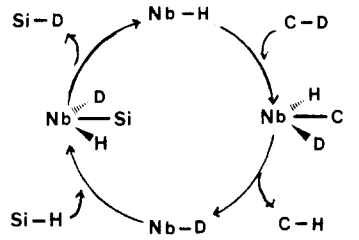

Nb = Cp_2Nb

Net: C–D + Si–H ⟶ C–H + Si–D

The transient peaks B, D, and E do not correspond with the known spectrum[9] of dimer **5** and may be due to intermediate silyl complexes or to "$[Cp_2NbH]_n$" species other than **5**. In a control experiment, it was shown that preformed dimer **5** is unreactive toward C_6D_6 or Et_3SiH. Therefore, the deuterium incorporation into **5** precedes its formation. Hence, there must be labile isomers of **5** in solution which are capable of exchanging Cp–H with C_6D_6. As these labile species are converted to unreactive **5**, the H/D exchange eventually halts. The *final* products are as shown in eq 10.

$$Cp_2NbH_3 + C_6D_6 + Et_3SiH \rightarrow \underset{n = 0\text{–}10}{\mathbf{5}\text{-}d_n} + \underset{20\text{–}50\%\ d_1}{Et_3SiH(D) + C_6D_5H} \quad (10)$$

We interpret the difference in behavior of $PhMe_2SiH$ and Et_3SiH toward H/D exchange with C_6D_6 as follows: $PhMe_2SiH$ forms the stable silyl adduct **3**, which does not insert into the C–D bonds of C_6D_6. Et_3SiH must form a labile adduct which is in equilibrium with Cp_2NbH, **6**. Compound **6** may insert directly into the C–D bond and undergo H/D exchange or may dimerize by insertion into a Cp–H bond.

An important question is: why are no phenyl silanes formed even though both the C–D and Si–H bonds are "activated" by the catalyst for H/D exchange? We believe the answer to this question lies in the stereochemistry of the oxidative addition adducts of **6**. In the silyl derivatives, the Si replaces the central hydrogen of Cp_2NbH_3. Although stable $Cp_2Nb(H)_2Ar$ complexes have not been isolated, it is reasonable to assume that the Ar group will also occupy the central position. Thus, the catalytic cycle shown in Scheme II will effect H/D exchange.

Productive C–H activation is not observed because the isomers **7** and **8** are not formed. These isomers could

7 **8**

Cp_2Nb–Ar Cp_2Nb–SiR_3

9 **10**

eliminate the cis hydrides as H_2 and form intermediates **9** and **10**, which may insert into Si–H or C–H bonds to give productive C–H activation (see eq 11). There is a general

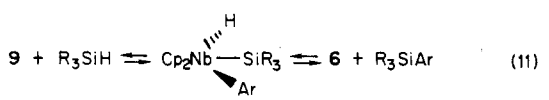

(11)

11

conclusion in all this: to get *productive* C–H activation, there must be not just three exchangeable sites on the metal, there must be 3 *mutually* exchangeable sites.

Ir(III) complexes, formed by oxidative addition of, e.g., R_3SiH to L_3IrH, are often facial (**12**). In complex **12**, all three exchangeable sites are mutually cis and mutually exchangeable in principle. This is one reason why Ir complexes are effective in promoting productive C–H activation.

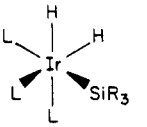

12

The conclusion that three mutually exchangeable sites are necessary for productive C–H activation has an important implication. In the general exchange reaction (eq 12), the active catalytic intermediate will form various

$$C\text{–}H + H\text{–}X \xrightarrow[M\text{–}H]{cat.} C\text{–}X + H_2 \quad (12)$$

species, e.g., $M(C)(H)_2$ and M(H)(C)(X), from sequences such as that shown in eq 13. The M(H)(C)(X) intermediate may "decompose" by three paths if all sites are mutually exchangeable (eq 14).

$$M\text{–}H + C\text{–}H \rightleftarrows MH_2C \overset{-H_2}{\rightleftharpoons} M\text{–}C \overset{HX}{\rightleftharpoons} M(H)(C)(X) \quad (13)$$

$$HX + MC \underset{(1)}{\rightleftharpoons} M(H)(C)(X) \begin{cases} \xrightarrow{(2)} M\text{–}H + C\text{–}X \\ \xrightarrow{(3)} M\text{–}X + HC \end{cases} \quad (14)$$

If one follows through all the possibilities, one sees that there are 10 M(III) intermediates for a metal cycling between oxidation states M(I) and M(III). These 10 intermediates may decompose into all possible products, e.g., for eq 12:

	C	H	X
C	C–C	C–H	C–X
H		H–H	H–X
X			X–X

For the specific case of eq 4, the expected products are Ph–Ph, Ph–SiR_3, H_2, and R_3Si–SiR_3 in addition to the starting materials Ph–H and R_3Si–H. In fact, depending on the catalyst, *all* these species have been found in the reaction mixtures.[5-8,23] Thus, if productive C–H activation is to be specific, a fortuitous combination of rates of formation and decomposition of the M(III) intermediates must be obtained. In this connection, only a few kilocalories per mole are required to shift the relative rates of the various decomposition paths shown in eq 14 a 100-fold.

Although the above analysis concentrated on C–H activation catalyzed by metals cycling between M(I) and M(III) oxidation states, the analysis holds for any catalyst system operating by oxidative addition/reductive elimination pathways.[24] By placing C–H activation under the

(23) Redistribution or exchange reactions involving R_3SiH are even more complex since Si–R bonds as well as Si–H bonds enter into the reaction sequence.

(24) An exception to this analysis is the case in which productive C–H activation occurs by migratory insertion, e.g., that in ref 3i. In this case, however, the excess addendum, e.g., CO, will tend to compete with the C–H bond for occupation of the vacant coordination site, thus blocking catalytic activity:

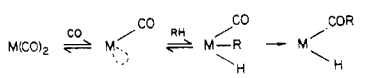

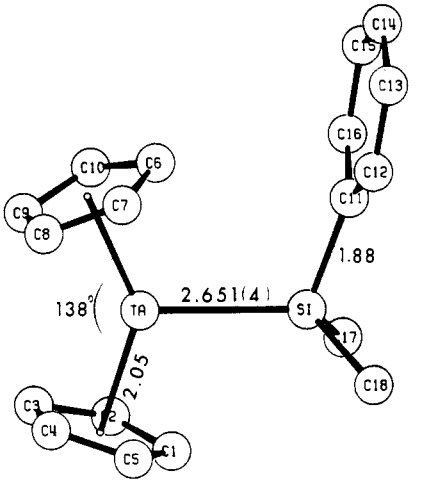

Figure 4. ORTEP plot and numbering scheme for $Cp_2Ta(H)_2SiPhMe_2$ (4).

general aegis of redistribution reactions, one sees that specific reactivity will be difficult to obtain in practice.

X-ray Structure of $Cp_2Ta(H)_2SiMe_2Ph$. Figure 4 shows the ORTEP plot of $Cp_2Ta(H)_2SiPhMe_2$ (4). The hydrogens bonded to the tantalum could not be located on the final difference map, but they undoubtedly flank either side of the Ta–Si bond. The two Cp rings are eclipsed and the Ta–Cp (ring centroid) distances are 2.036 (7) and 2.070 (7) Å. The Cp–Ta–Cp angle is 138.0 (2)°. These values are common for Cp_2TaX_3 structures.[10]

The $SiPhMe_2$ ligands adopts a conformation in the solid state which gives the molecule nearly strict C_s symmetry (there is no crystallographic symmetry). The hydrogen attached to C_6 appears to point toward the center of the phenyl ring bonded to silicon. However, the ^1H NMR shows that in solution there is rapid rotation about the Ta–Si bond. Hence, the conformation of 4 seen here must be only a few kilocalories per mole more stable than alternate rotomeric conformations.

The principal noteworthy feature of this structure is the Ta–Si bond length, 2.651 (4) Å. We are not aware of any other structurally characterized Ta–Si compounds, but an expected Ta–Si bond length may be derived from the Ta–C and Si–C bond lengths. The $Ta–CH_3$ distances in $Cp_2TaMe(=CH_2)$ is 2.246 (12) Å, and the $Ta–CH_2$ distance in $Cp_2Ta(CH_2Ph)(=CHPh)$ is 2.30 Å.[25] The average of these two values is about 2.27 Å. Subtracting the radius of carbon (0.77 Å) gives 1.50 Å as the expected radius for Ta in Cp_2Ta derivatives. The silicon radius (1.11 Å) is derived from the observed Si–C distance of 1.88 Å. Thus, the expected Ta–Si distance is 1.50 + 1.11 = 2.61 Å, so the observed Ta–Si bond distance would not appear to be unusual for a Ta–Si single bond.

This only previously reported bond length between silicon and a heavy, early transition metal is 2.813 (2) Å for the Zr–Si bond in $Cp_2Zr(Cl)SiPh_3$.[26] This distance is about 0.2 Å longer than that expected on the basis of covalent radii. Bonds between Si and electron-rich metals, e.g., groups 8–10,[28] are shorter than the sum of the covalent radii. This shortening has been ascribed to the effects of $d_\pi–d_\pi$ bonding which is absent in the d^0 metals. (The Nb–Sn bond length in $Cp_2Nb(CO)SnX_3$, a d^3 system, is also considerably shorter than the sum of the respective covalent radii.[27])

The "normal" Ta–Si distance found for 4 suggests that $M(d^0)$–Si bonds are not inherently weak. In $Cp_2Zr(Cl)SiPh_3$, the bulky Ph_3Si group lies to one side of the Cp–Zr–Cp (Cp = ring centroid) plane, i.e., toward the closed portion of the bent sandwich, and steric factors may stretch the Zr–Si bond. In 4, the $PhMe_2Si$ group is bonded to the most open position of the Cp_2Ta fragment and there are no steric problems.

Acknowledgment. We thank the Office of Naval Research for support of this research.

Registry No. 1, 11105-67-2; 2, 12117-02-1; 3, 94930-01-5; 4, 94930-02-6; Cp_2NbCl_2, 12793-14-5; Cp_2TaCl_2, 54039-37-1; $CpNbCl_4$, 33114-15-7; $CpTaCl_4$, 62927-98-4; EDE, 107-51-7; E′DE, 2895-07-0; $E'D_2E$, 17478-07-8; $E'D_3E$, 17066-04-5; $CpNb(H)_2(SiMe_2OSiMe_3)$, 94943-95-0; $PhMe_2SiD$, 22034-19-1; Et_3SiD, 1631-33-0; C_6D_5H, 13657-09-5; Bu_3SnCp, 94930-04-8; $NbCl_5$, 10026-12-7; $TaCl_5$, 7721-01-9; $PhSiMe_2H$, 766-77-8; Et_3SiH, 617-86-7; pentamethyldisiloxane, 1438-82-0.

Supplementary Material Available: Table IV, thermal parameters (U_{ij}) for 4, and Table VI, F_o vs. F_c for 4 (12 pages). Ordering information is given on any current masthead page.

(25) Guggenberger, L. J.; Schrock, R. R. *J. Am. Chem. Soc.* **1975**, *97*, 6578. Schrock, R. R.; Messerle, L. W.; Wood, C. D.; Guggenberger, L. J. *Ibid.* **1978**, *100*, 3793.

(26) Muir, K. W. *J. Chem. Soc. A* **1971**, 2663.

(27) Shripkin, Yu. V.; Volkov, O. G.; Pasynskii, A. A.; Antsyshkina, A. S.; Dikaveva, L. M.; Ostrikova, V. N.; Porai-Koskits, M. A.; Devydova, S. L.; Sakharov, S. G. *J. Organomet. Chem.* **1984**, *263*, 345.

(28) The group notation is being changed in accord with recent actions by IUPAC and ACS nomenclature committees. A and B notation is being eliminated because of wide confusion. Group I becomes groups 1 and 11, group II becomes groups 2 and 12, group III becomes groups 3 and 13, etc.